3D implicit stratigraphic model building from remote sensing data on tetrahedral meshes: theory and application to a regional model of La Popa Basin, NE Mexico.

Guillaume Caumon, Gary Gray, Christophe Antoine, Marc-Olivier Titeux.

***Abstract*—Remote sensing data provide significant information to constrain the geometry of geological structures at depth. However, the use of intraformational geomorphologic features such as flatirons and incised valleys often calls for tedious user interaction during 3D model building. We propose a new method to generate 3D models of stratigraphic formations, based primarily on remote sensing images and digital elevation models. This method is based on interpretations of the main relief markers and interpolation of a stratigraphic property on a tetahedral mesh covering the domain of study. The tetrahedral mesh provides a convenient way to integrate available data during the interpolation while accounting for discontinuities such as faults. Interpretive expert input may be provided through constrained interactive editing on arbitrary cross-sections and additional surface or subsurface data may also be integrated in the modeling. We demonstrate this global workflow on a structurally complex basin in the Sierra Madre Oriental, Northeastern Mexico.**

***Index Terms*—G.1.1Interpolation G.1.6:Optimization G.1.10:Applications G.2.3: Applications H.5.2:Graphical User interface I.2.1.a:Cartography I.6.5: Model development J.2.e Earth and atmospheric sciences J.6.a Computer-aided design**

I. Introduction

Multispectral satellite imaging provides valuable information in geological mapping thanks to exhaustive imaging between the formation boundaries. Indeed, images can be projected onto digital elevation models to create a digital terrain model (DTM), then used by geomophologists to interpret the orientation of 3D features such as flatirons, cuestas and incised valleys. Such landform analysis and stereoscopic imaging tell much about geological structures [1], [2] and dynamic changes to the earth surface [3], [4]. At a higher resolution, LIDAR mapping also provides much detail about geological features observed on outcrop, including both accurate geometry, laser intensity and color to help automated identification and characterization of geological bodies [5], [6].

The use of such exhaustive surface data for subsurface description is attracting more and more interest in the geoscience community, due in particular to progresses in obtaining accurate surface geometry from remote rensing data [3], [4], [7]. However, most 3D geomodeling methods are designed to use dense data as obtained from 3D seismic surveys. In the case where surface data form the bulk of observations, many systems provide tools to generate a stratigraphic model using layer thickness maps and / or projections, possibly constrained by interpretive cross-sections [8], [9]. Such methods are generally effective in simple geological settings but cannot easily represent all geological structures encountered in nature, for example overhangs due to salt or overturned folds and structures affected by inverse faults. Alternatively, truly three-dimensional systems usually define a set of consistent 3D surfaces bounding geological volumes. This type of method has been used successfully to generate 3D models from field and remote sensing data [1], [2], [10]–[16].

A first challenge with most earth surface data is the very strong anisotropy of information density: on the topographic surface data are extremely dense whereas subsurface data are much sparser. In stratigraphic settings, most existing workflows iteratively build major stratigraphic horizons from their trace on the topography and either ignore or express intraformational observations between main horizons in a way that can be understood by

G. Caumon and Christophe Antoine are with the Centre de Recherche Pétrographiques et Géochimiques (UPR-2300 CNRS) and with the Université de Lorraine-ENSG, F-54501 Vandoeuvre-Lès-Nancy (e-mail:Guillaume.Caumon@univ-lorraine.fr; antoine@gocad.org).

G. Gray is with ExxonMobil Upstream Research, Houston, TX 77252.

M.-O. Titeux was with the Centre de Recherche Pétrographiques et Géochimiques (UPR-2300 CNRS) and the Université de Lorraine-ENSG. He is now with IFPEnergies Nouvelles, F-92852 Rueil-Malmaison.

Manuscript received Dec. 22, 2010 ; Accepted June 24, 2012

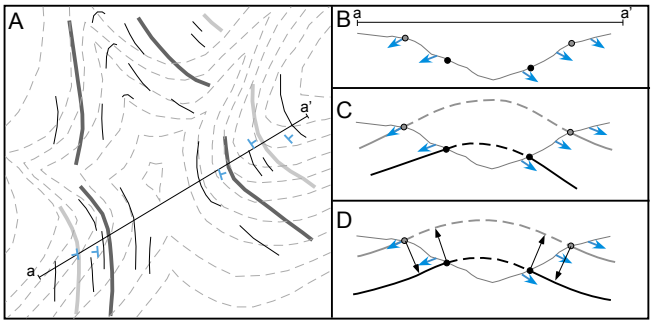

Fig. 1. Typical information derived from remote sensing data to constrain 3D geological models, and possible modeling strategy. A: Map view of major stratigraphic horizons (bold grey lines), strike and dip measurements (blues T's) and intraformational stratigraphic lineations (black lines) interpreted on a topographic surface (dashed elevation curves). B-D: possible modeling procedure shown on the a-a' cross-section, modified from [17]. In C, individual horizons are created from horizon lines and orientation measurements (blue arrows). In D, layer thicknesses are iteratively computed and used to refine the model. In this process, many stratigraphic lineations must be discarded because they do not clearly define a plane.

the 3D modeling system. To-date, these intraformational observation points only consist of stratigraphic orientation points. These points are often projected onto the base or the top of the layer [11], [13], [14]. Alternatively, dip domains of constant orientation based on structural analysis and mapping of axial surfaces can be used [2], [12]. Further, Salles et al. [17] estimate thickness maps and use projections to and from layer boundaries to iteratively refine the 3D model (Fig. 1). The main benefits of the latter approach are that it corrects for non-representative sampling of the various geological surfaces on the topography and controls the extrapolation of subtle thickness and orientation changes in growth strata. However, such specific modeling methodologies generally involve time-consuming manipulations by the modeling expert; surface data are generally complemented by 2D interpretive cross-sections, which often need to be edited because inconsistencies with neighboring data occur. Additionally, data need to be projected onto the geological surfaces during the modeling process, which introduces errors when layer thickness varies or when the projection direction crosses a fault. The method presented in this paper directly builds 3D stratigraphic volumes, as proposed previously [18], [19]; this removes the need for projecting data points onto surfaces, and directly exploits coherency between successive conformable horizons.

A second challenge with remote sensing data lies in the way orientation data are obtained. Indeed, orientations measured in the field are not necessarily reliable for building regional scale models, because small local features may be measured instead of regional trends [2]. Stratigraphic orientation may be computed from stereoscopic images [1], but this involves significant manual work and can only provide a limited number of points. Alternatively, stratigraphic contacts may be picked or detected on a DTM to rapidly produce a much denser set of input data [20]. However, georeferencing errors or limited DEM resolution may introduce approximations. Even with consistent input, the orientation is poorly constrained when the bedding lines are almost straight. To improve the quality of the orientation data, error metrics have been proposed to characterize the shape of the covariance ellipsoid computed locally over line point coordinates [2]. Based on these metrics, prolate and spherical ellipsoids indicative of poor orientation estimates can be discarded. While this stategy eliminates noisy data, it also discards informative straight lines from subsequent modeling steps. For instance, the lines shown on Fig. 1-A may all be considered too straight or noisy to provide a reliable estimate of stratigraphic orientation. However, a trained geologist can readily identify the NNW/SSE axial direction of the anticline by looking at ALL stratigraphic contacts at once.

In this paper, our objective is to address these two challenges by considering geological surfaces as level sets of an underlying scalar field. Such an implicit modeling method takes all data points at their exact location and provides a built-in volumetric consistency, which facilitates 3D geological modeling (Section II). In the proposed approach (Section III), we introduce a way to directly constrain the 3D geometry by stratal traces interpreted on a DTM, without intermediate and potentially unstable orientation computation (Section III-B). This methodology can be applied to generate a regional 3D model using satellite data only, but additional field data, borehole data, interpretive cross-sections and seismic lines may also be incorporated (Section III-D). In Section IV, we describe an application of this method to La Popa Basin in the Sierra Madre Oriental, Mexico.

II. Background: Implicit Geological Modeling

Implicit or level set methods consider geological interfaces as equipotential surfaces of a 3D scalar field. This approach is becoming more and more popular for geological modeling, because computational power now makes it possible to efficiently generate this scalar field while honoring available data [18], [21]–[24]. Two main types of methods have been described to create such scalar fields from field and subsurface data:

- Dual kriging and radial basis function interpolation

provide an estimation of the scalar field f as:

$$f(\mathbf{x}) = \sum_{l=1}^{L} c_l \cdot p_l(\mathbf{x}) + \sum_{n=1}^{N} \lambda_n \cdot \phi(|\mathbf{x} - \mathbf{x}_n|) \quad , \quad (1)$$

where $p_l(\mathbf{x})$ are polynomial basis functions, c_l the corresponding drift coefficients, and L the total number of polynomial terms; N is the total number of data points; $\phi(|\mathbf{x}-\mathbf{x}_n|))$ is either the covariance between the data point $\mathbf{x}_n$ and the unknown $\mathbf{x}$ [25] or a basis function such as a thin plate spline or simply the distance (also called biharmonic function) [26]; λ_n are the unknown interpolation coefficients. Finding the coefficients of eq. (1) requires solving a dense linear system of the form [25], [26]:

$$\begin{bmatrix} \mathbf{\Phi} & \mathbf{P} \\ \mathbf{P}^T & \mathbf{0} \end{bmatrix} \cdot \begin{bmatrix} \lambda \\ \mathbf{c} \end{bmatrix} = \begin{bmatrix} \mathbf{f} \\ \mathbf{0} \end{bmatrix} \quad (2)$$

where

$$\mathbf{\Phi} = \begin{bmatrix} \phi(0) & \cdots & \phi(|\mathbf{x}_1 - \mathbf{x}_N|) \\ \vdots & \ddots & \vdots \\ \phi(|\mathbf{x}_N - \mathbf{x}_1|) & \cdots & \phi(0) \end{bmatrix}$$

and

$$\mathbf{P} = \begin{bmatrix} p_1(\mathbf{x}_1) & \cdots & p_L(\mathbf{x}_1) \\ \vdots & \ddots & \vdots \\ p_1(\mathbf{x}_N) & \cdots & p_L(\mathbf{x}_N) \end{bmatrix}.$$

This system can be used to build implicit surfaces from point clouds [26], [27]. For this, data points are duplicated and projected along the locally computed surface normal; Eq. (2) is then solved by taking ϕ as the identity function (*i.e.*, the basis functions in Eq. (2) are simply the Euclidean distances $|\mathbf{x} - \mathbf{x}_n|$). When the number N of data points increases, the $O(N^2)$ size of the (dense) system (2) makes it impossible to be inverted with standard techniques. Therefore, [26] proposed using a $O(N)$ multigrid numerical method called the fast multipole method, initially proposed for computing the interaction of charged particles [28]. This method is convenient to construct continuous and smooth geological shapes [27], but application to faulted formations remains unclear.

A combination of scalar fields can be used to represent more complex structures, including stratigraphic unconformities and faults [19]. The set of fields is computed with dual kriging (1) and a special iso-surface extraction method based on the Marching cubes [29]. The interpolation is achieved by dual kriging of the difference between the scalar field and some arbitrarily fixed reference value, as initially proposed in 2D [21] and later extended to 3D [22]. As compared to radial basis functions, this formulation of dual kriging of increments is well suited to honor orientation data. Moreover, known faults can be accounted for through discontinuous polynomial drift coefficients and borehole ends through inequality constraints implemented by a Gibbs sampler [19], [22]. However, to our knowledge, this method is limited by the amount of input information points: the fast multipole method has not been applied to dual kriging with such a diverse set of constraints (gradient data and inequality constraints). Also, interactive editing is not direct since the addition of an interpretive data point requires building and solving the whole system again.

- Alternatively, the scalar field may be computed by discrete optimization on some pre-defined volumetric mesh. For example, a Euclidean distance field can be computed on a Cartesian grid to reconstruct complex surfaces, but faults can then be treated only up to the grid resolution [30]. This scalar field may also be computed on tetrahedral meshes conforming to faults by solving a linear system of M unknowns $f_1, \ldots, f_M$ at the mesh nodes [18], [23]:

$$\mathbf{A} \cdot [f_1 \cdots f_M]^T = [b_1 \cdots b_C]^T = \mathbf{b}^T \quad , \quad (3)$$

where C is the total number of linear constraints applied to the system; the coefficients of these constraints are stored in the $C \times M$ sparse matrix $\mathbf{A}$ and the right-hand side vector $\mathbf{b}$. In general, Eq. (3) includes a term to obtain smooth isosurfaces, and additional boundary conditions to account for observations [18], [31], leading to an overdetermined system which can be solved in the least-squares sense using the conjugate gradient algorithm. As compared to splines and dual kriging, this method requires a 3D mesh to be defined before computing the scalar field. The time needed to solve the system depends primarily on the size of the mesh and marginally on the number of data points [18]. Such a model-centric vision is interesting in geological modeling because model resolution is controlled not by data layout, which is generally irregular in geosciences, but by mesh density [16]; resolution may also be locally modified to keep a low discrepancy between data and interpolated geometry [18]. Local model updating can be achieved in real-time by interpolating only around selected interpretive data points.

III. Interpolation of a stratigraphic function from remote sensing-based interpretations

A. Proposed methodology

The proposed methodology starts with georeferenced geometric data interpreted on Digital Terrain Models or Digital Outcrop Models (DOMs). For clarity, we will describe the procedure to build the 3D geometry of a conformable stratigraphic sequence. The adaptation of the method to faults and unconformities will be discussed in Section III-C. Three data types are considered jointly by the method:

- 3D lines corresponding to the surface traces of known stratigraphic horizons, possibly interpreted in conjunction with actual field observations or 2D geological maps.
- 3D lines representing intraformational stratal traces, without knowledge of stratigraphic age.
- Bedding orientation measurements obtained from field measurements and/or orthophotogrammetry [1].

The domain of study is then filled with a tetrahedral mesh. In our implementation, we use either the commercial tetrahedral mesher of the Gocad software [32] or the free tetgen code [33], both of which allow for adapting the mesh resolution to the desired level of detail.

The linear system (3) is then built depending on the data at hand (Section III-B), and solved in the least-squares sense. For quality control, the main horizons are extracted from linear tetrahedra. The geometry of stratigraphic boundaries can be interactively edited on cross-sections or iso-surfaces; elementary model validity rules [34] are observed throughout editing. This implicit stratigraphic model may then be restored sequentially and decompacted for palinspastic reconstruction using a mechanical finite element method [35], [36].

B. Building the linear system

Our goal is to express all data types corresponding to remote sensing interpretations as linear equations fed to the system (3). As proposed by Frank et al. [18], we consider a linear tetrahedron, whereby the gradient ∇f of the scalar field f is uniquely defined from the values f_i of f at the four vertices (x_i, y_i, z_i) of the tetrahedron $(i = 1, \ldots, 4)$:

$$\nabla f = \begin{bmatrix} x_2 - x_1 & y_2 - y_1 & z_2 - z_1 \\ x_3 - x_1 & y_3 - y_1 & z_3 - z_1 \\ x_4 - x_1 & y_4 - y_1 & z_4 - z_1 \end{bmatrix}^{-1} \cdot \begin{bmatrix} f_2 - f_1 \\ f_3 - f_1 \\ f_4 - f_1 \end{bmatrix} \quad (4)$$

In the implicit framework, points defining the position of a known stratigraphic horizon must all have the same value. In practice, this value may correspond to the age of the horizon [37], or preferably to a relative average thickness from a reference horizon. Then, a point $\mathbf{p} = (x_p, y_p, z_p)$ of known scalar value f_p, can be honored by adding the following line to the system (3) [18]:

$$\sum_{i=1}^{4} u_i \cdot f_i = f_p \quad , \quad (5)$$

where f_i are the (unknown) scalar values at the vertices of the tetrahedron containing the point $\mathbf{p}$, and u_i the barycentric coordinates of $\mathbf{p}$ the tetrahedron.

Accounting for an orientation datum $\mathbf{p}$ is best achieved by using the strike vector $\mathbf{s}_p$ and the dip vector $\mathbf{d}_p$ at $\mathbf{p}$. By definition, an implicit stratigraphic surface honors this orientation information if the gradient of the scalar field ∇f at point $\mathbf{p}$ is orthogonal to both $\mathbf{s}_p$ and $\mathbf{d}_p$. Therefore, this equation is discretized in the the tetrahedron containing $\mathbf{p}$ by substituting Eq. (4) in:

$$\begin{cases} \nabla f \cdot \mathbf{s}_p &= 0 \\ \nabla f \cdot \mathbf{d}_p &= 0 \end{cases} \quad (6)$$

As we have seen, orientations obtained from DTMs or DOMs may not be reliable. Therefore, it is also possible to directly account for polygonal curves representing stratigraphic lineations. Indeed, an implicit stratigraphic surface honors a lineation as long as the gradient of the scalar field ∇f is orthogonal to that lineation. For each line segment of direction $\mathbf{l}$ crossing a tetrahedron over a length w, the equation:

$$w \nabla f \cdot \mathbf{l} = 0 \quad (7)$$

can be added the system (3). Although the term w may seem unnecessary when looking at Eq. (7), it should be conserved in the the global system (3) because it provides relative weighting of all lineations independently of their sampling and of the mesh resolution. When two polygonal line segments of directions $\mathbf{l}_1$ and $\mathbf{l}_2$ cross a tetrahedron, the gradient of the scalar field tends to orient orthogonally to both of them, and is strictly equivalent to Eq. (6) when segments are orthogonal and have the same length in the tetrahedron.

In addition to these data terms, a smoothness regularization term should also be added to the system (3). For this, two strategies have been described previously. One is to minimize the integral of $||\nabla f||$ over the whole domain by analogy with work minimization in an isotropic diffusive problem [31].

In our work, we use the approach of [18] which minimizes the curvature of implicit surfaces defined

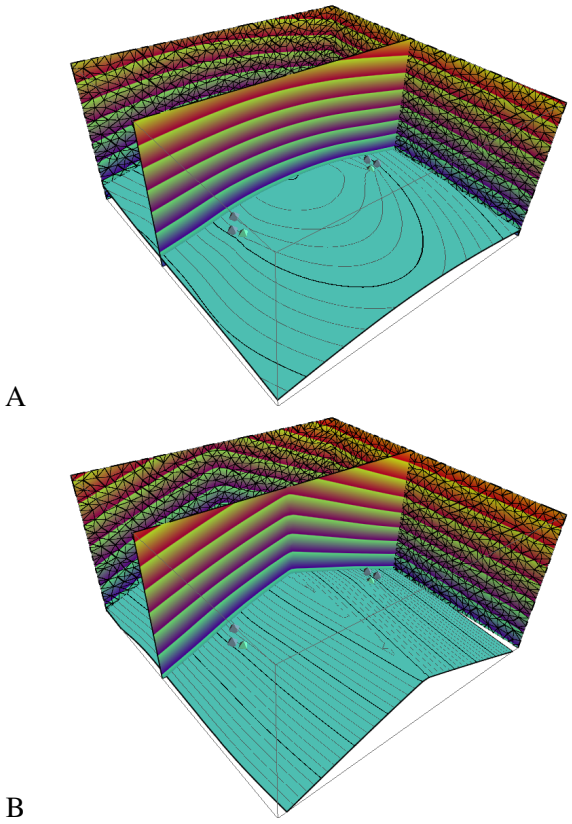

Fig. 2. Interpolation results with dip domains on a simple synthetic example. A: only a global smoothness term (Eq. (8)) was used on top of sparse horizon data, displayed as diamonds (Eq. (5)). B: Two dip domain regions were created on both sides of the axial surface, and local roughness terms were added in these regions. The weight ratio between global smoothness vs. local smoothness was set to 1/100.

by the scalar field f. This term is discretized on all internal faces of the tetrahedral mesh so that the variation of gradient $(\nabla f^{\diamond} - \nabla f^{\star})$ between any two adjacent tetrahedra $\mathcal{T}^{\diamond}$ and $\mathcal{T}^{\star}$ is constrained to be null. Because three nodes are shared by both tetrahedra, this difference can be projected without loss of information onto the normal $\mathbf{N}$ to the common face between $\mathcal{T}^{\diamond}$ and $\mathcal{T}^{\star}$ before being added to the system (3):

$$(\nabla f^{\diamond} - \nabla f^{\star}) \cdot \mathbf{N} = 0 \tag{8}$$

In our implementation, this smoothness term (8) can be computed on dip domain regions of the tetrahedral mesh to allow for additional structural input, as in [12]. In this case, the relative weight between the global smoothness and local smoothness controls the degree of sharpness of fold hinges (Fig. 2).

C. Handling discontinuities

As compared to general-purpose 3D modeling applications, the management of discontinuities is essential in geological modeling. We will now explain how the proposed method can be applied to domains with faults, salt welds and unconformities. As proposed also by [19], unconformities can be handled by using several scalar fields for all conformable rock units. Each unit is defined by a scalar field and lower and upper bounds; boolean operations are then performed between units depending on the type of unconformity. By construction, this approach extrapolates eroded units above unconformities, thereby providing a first estimate of the amount of eroded material. This observation can be used later on for palinspastic reconstructions as proposed by [35], [36].

Faults and salt welds can be treated as implicit surfaces with exactly the same constraints as for stratigraphy. In this case, the scalar field values on the data are arbitrarily set to 0; the convergence of the system is ensured by adding a local orientation constraint specifying the average plane of the data points. For this, we do not use Eq. (6) but strictly identify the gradient of the scalar field ∇f with the normal to the average plane $\mathbf{n}_p$ (where $\mathbf{n}_p = \mathbf{s}_p \times \mathbf{d}_p$):

$$\nabla f = \mathbf{n}_p \tag{9}$$

This point is chosen to be far from the discontinuity data to minimize artifacts. As a result, the scalar field provides an estimate of the signed distance to the discontinuity everywhere in the volume. Then, after visual control, the tetrahedral mesh can be cut by the 0-isosurface corresponding to the discontinuity. For synsedimentary faults and faults with lateral termination, the areal extent of the fault can be defined in a 3D region to bound the cut operation. Contacts between discontinuities are recovered by applying this procedure iteratively, by considering major faults before branching faults [38]. One drawback of this strategy is that the tetrahedral mesh quality decreases as the mesh is cut by discontinuities, which may cause problems for applications of 3D restoration with the finite element method (FEM). Therefore, another possibility is to obtain explicit discontinuity surfaces and re-mesh the volume of interest conformably to these surfaces [33].

D. Model editing

When building models from surface data, expert model editing is often necessary to increase the quality of the extrapolation at depth. This task is difficult when dealing with explicit triangulated surfaces, because significant processing is needed to keep model integrity [34]. A major advantage of the implicit method, also pointed out by [18], [19], [31] is that model updating is much easier than with explicit surfaces. In our case, new points or lines may be added and moved interactively at

Fig. 3. Satellite picture (Landsat Thematic Mapper) of La Popa Basin.

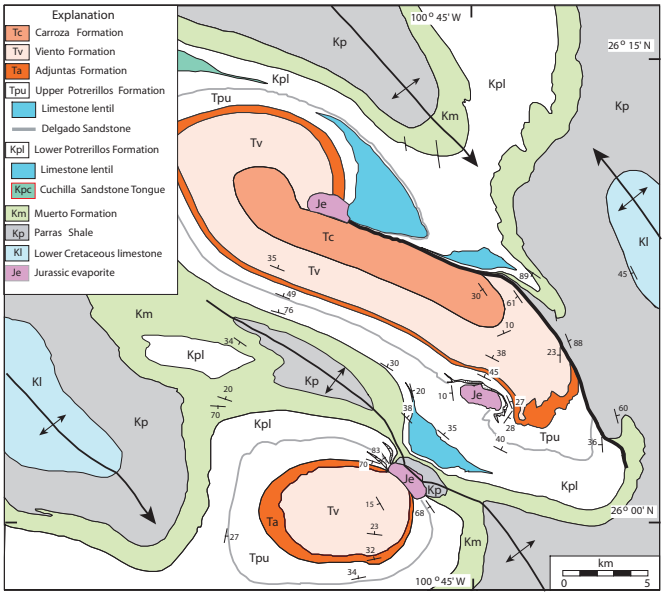

Fig. 4. Geological map of la Popa Basin (modified from [43]).

depth to control the geometry of a particular implicit surface. As proposed by [18], [39], these interpretive points are added as new terms in the linear system (3) using Eq. (5), and the system is solved from the current state. Updating may also be done locally around the interpretive points to increase performance. It is then possible to update the model and provide visual feedback as points are moved by the user.

Interactive editing of faults is more difficult, because in the end faults are represented explicitly in the tetrahedral mesh. For small geometric changes, it has been proposed to distort the mesh while minimizing the variation of volume during deformation [39]. For larger changes, however, the model must be completely rebuilt.

IV. Application: Modeling of La Popa Basin, Nuevo Leon, Mexico

La Popa Basin lies in the Sierra Madre Oriental, and is part of the Laramide fold and thrust belt in North America. This basin displays ample folds affecting Lower Cretaceous to Eocene formations (Fig. 3 and 4). Outcrop conditions are excellent, which makes the area an excellent candidate to use remote sensing data for geological interpretations [40], [41]. This basin is remarkable because it contains three salt diapirs, called El Gordo, El Papalote and La Popa diapirs. Also, a former salt escape conduit (weld) can be identified in the basin trending SE from the la Popa diapir along an azimuth of approximately 135 [42]. Although field observations show evidence of many interesting geometric features around this salt weld [41], [43], at the basin scale, the weld could be mistaken for (and has been modeled as) a fault. Salt movements are interpreted as major influences on the structural and depositional evolution during the Late Cretaceous and Eocene.

In the first step of the modeling, a 44km by 35km Landsat Thematic Mapper image and the 3 arc-second STRM digital elevation model (DEM) were imported into the Gocad geomodeling software. The image was georeferenced from a set of corresponding points recognizable both on the DEM and on the satellite image as geomorphologic features.

Next, three stratigraphic horizons were chosen, corresponding to the base of the Muerto, Delgado and Viento Formations, and a set of polygonal lines representing intersections between stratigraphic surfaces and the topography was created (Fig. 5). The picking of these lines was made from geomorphologic features, aiming at maximizing the geometric significance of the lines to define the orientation. For this, we followed winding paths on flatirons when possible, as shown on the detailed view in Fig. 5.

The data described above have been used as input to the implicit stratigraphic modeling method described in Section III. Volumetric modeling was performed both above and below the present topographic surface on an isotropic mesh consisting of 122K tetrahedra corresponding approximately to a 600m resolution. The model covers elevations between -5,500 and 8,000m. For convenience, the salt was ignored in this regional model; however, the salt weld has been extrapolated vertically, and used to cut the tetrahedral mesh. This was motivated by the obvious termination of some stratigraphic markers in the neighborhood of the weld,

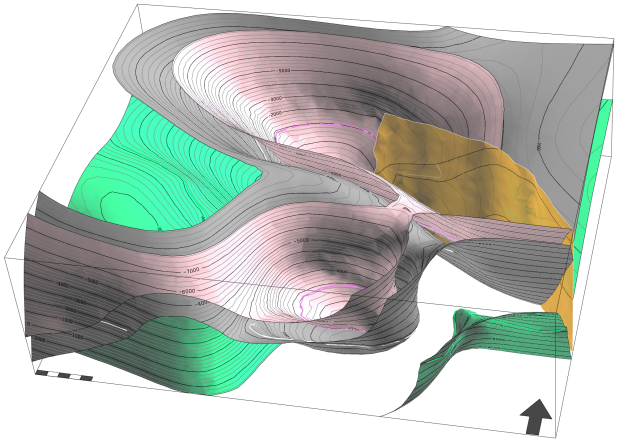

A: Muerto, Delgado and Viento horizons build from corresponding traces only

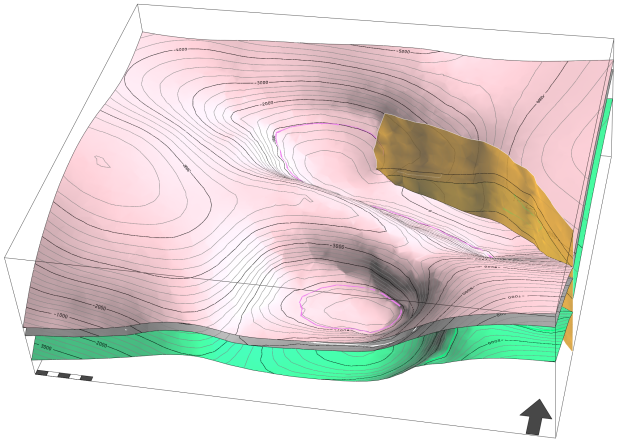

B: Muerto, Delgado and Viento horizons built from all stratal traces

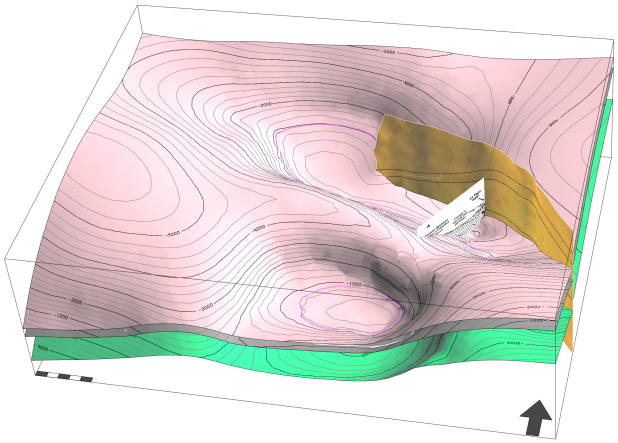

C: Muerto, Delgado and Viento horizons in the final model

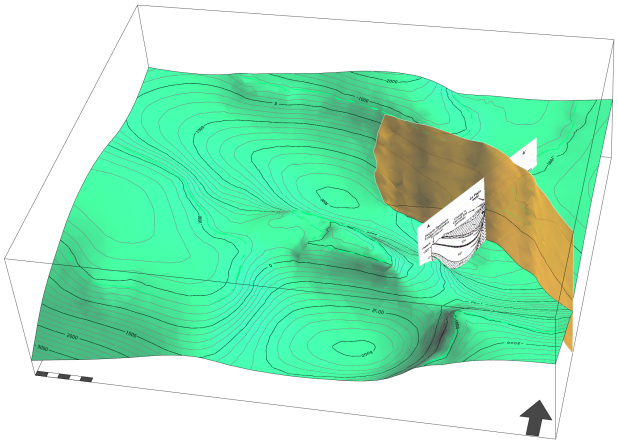

D: Muerto horizon in the final model

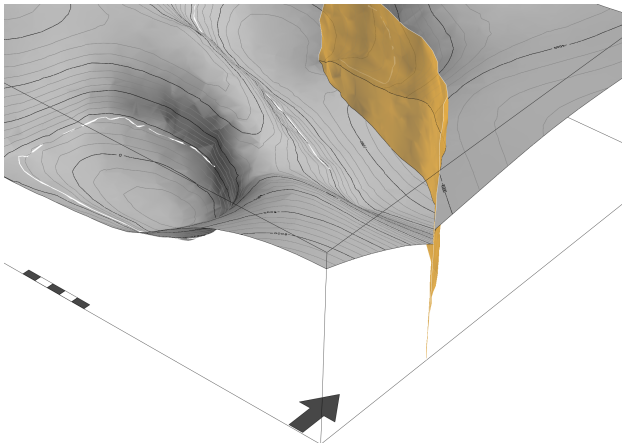

E: Detailed view of the Delgado horizon before adding the interpretive cross-section

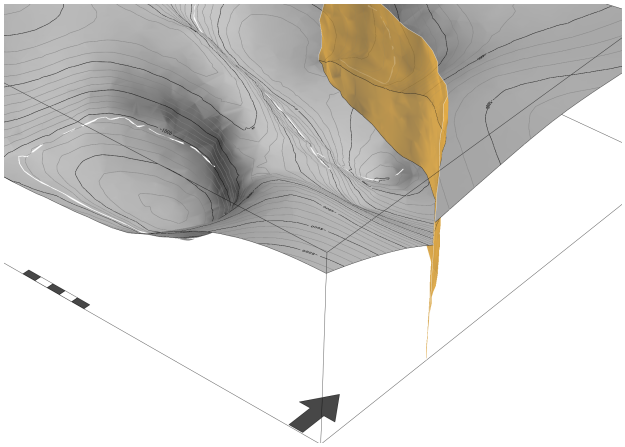

F: Detailed view of the Delgado horizon in the final model

Fig. 6. Views of the 3D model obtained using the implicit reconstruction method. See text for details.

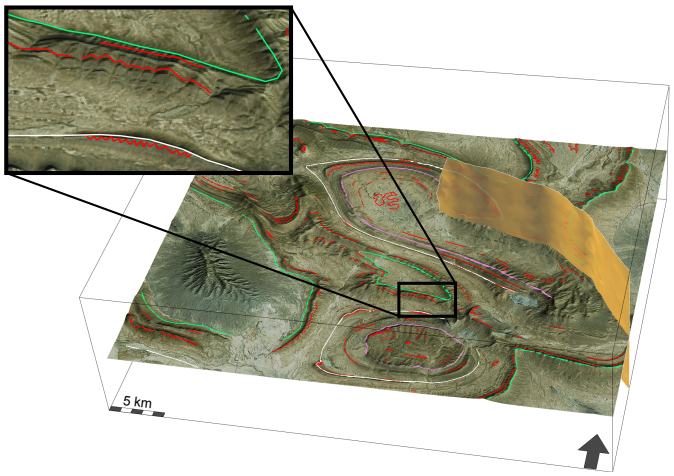

Fig. 5. 3D view of interpreted contours, stratal traces and salt weld on the digital terrain model. Picked lines correspond to the base of the Muerto Formation in green, the Delgado Sandstone in white and the base of the Viento Formation in pink. Other stratal traces, in red, were picked on flatirons and incised valleys when possible. Salt weld has been extrapolated vertically on the total model height.

indicating a significant stratigraphic offset. The scalar values for the three interpreted horizons were chosen as $1,000$ for the base of the Muerto Formation, $1,750$ for the Delgado Sandstone, and $2,000$ for the base of the Viento Formation, reflecting the average stratigraphic thicknesses between these horizons.

Using map traces of the three reference formations only generates horizons much steeper than actually observed (Fig. 6-A). This is due to the sparsity of data in 3D space and to the isotropic nature of the smoothness term (8). Adding intraformational stratal traces better contrains the dip of the model (Fig. 6-B,E). The maximum stratigraphic offset of the salt weld is then equal to 5,000m, which is consistent with previous studies [42], [43]. However, surface data do not allow to characterize the syncline on the hanging wall of the salt weld. Therefore, the model was further constrained by adding an interpretive cross-section line from Gile and Lawton [42] (Fig. 6-C,D,F). The final model is also available in the supplementary PDF3D file.

In terms of performance, the tetrahedral mesh construction and cutting by the salt weld took less than 5 minutes on a consumer laptop PC. Solving the linear system (3) was performed in less than a minute. Therefore, the most time-consuming work is the manual picking of stratal traces on the DTM, which is estimated to a few hours.

V. Conclusions and perspectives

We have presented a methodology to create 3D stratigraphic models from remote sensing data. As compared to previous work, data are taken into account at their exact location and do not need to be projected onto horizon surfaces. This facilitates the management of non-vertical faults and is has the potential to provide a fine control on the 3D geometry of growth strata. As compared to previous implicit modeling methods, this approach uses all interpretive data without prior computation of stratigraphic orientations or manual fitting. This allows for using all interpreted stratal traces at once, even if they poorly control the strike and dip of layers.

This method has the same limitations as previous work with regard with accuracy of input data. In particular, lines picked on a DTM may be sensitive to a difference of resolution between satellite or aerial image and the elevation model. In any case, lines should be picked carefully in a 3D graphics environment to avoid artifacts. In general, limited resolution of the elevation model also leads to underestimations of layer dip; recent methods which obtain an accurate elevation model at the pixel resolution [4], [7] should definitely help resolving these problems. Future work should take advantage of automated feature selection [44], [45] to provide better quality input lines to the method, or conversely, could use the reconstructed 3D model to further guide image analysis [3], [46].

At basin and regional scales, additional levels of detail may be integrated about the stratigraphy (e.g., through the the use of a high resolution stratigraphic column and several scalar fields [19]) and about the fault network. This could be challenging with hight level of detail or larger areas because of limitations in mesh generation and available computer memory. Hnagement of resolution is therefore an important avenue for further research. Also, significant uncertainty may exist in the 3D geometry due to noise of the remote sensing device or occusion problems [3]. Even if the method accounts for additional subsurface data (borehole information, seismic surveys) to constrain identified objects at depth, 3D subsurface geometry can never be determined withtout ambiguities because of lack of information. Therefore, we are also working on a stochastic extension of method able to generate and screen several possible 3D geometries [38], [47].

In the la Popa case study, we have focused on first-order features and ignored salt diapirs to keep the mesh size reasonable. The inclusion of the diapirs could be appropriate for more detailed modeling including also field data. Halokinetic sequences [43] are indeed clearly visible on the field, and 3D modeling coupled with restoration [35] could provide valuable insights into the interplay between salt movement and sediment architecture.

VI. Acknowledgements

We thank Exxonmobil for authorization to publish this work and the members of the Gocad Research Consortium for supporting this work, especially Paradigm for providing the Gocad software and API. We also acknowledge previous work from Jean-Laurent Mallet, Tobias Frank, Rémi Moyen and Anne-Laure Tertois who wrote part of the code used in this project. Thanks to Mary Ford and two anonymous reviewers for their comments and corrections. This is CRPG-CNRS contribution 2163.

References

[1] F. Bilotti, J. H. Shaw, and P. A. Brennan, "Quantitative structural analysis with stereoscopic remote sensing imagery," *AAPG Bulletin*, vol. 84, no. 6, pp. 727–740, Jun. 2000.

[2] O. Fernández, S. Jones, N. Armstrong, G. Johnson, A. Ravaglia, and J. Muñoz, "Automated tools within workflows for 3D structural construction from surface and subsurface data," *Geoinformatica*, vol. 13, no. 3, pp. 291–304, Sep. 2009.

[3] D. Crispell, J. Mundy, and G. Taubin, "A variable-resolution probabilistic three-dimensional model for change detection," *IEEE Trans Geosci Remote Sensing*, vol. 50, no. 2, pp. 489–499, Feb. 2012.

[4] M. Koga and A. Iwasaki, "Improving the measurement accuracy of three-dimensional topography changes using optical satellite stereo image data," *IEEE Trans Geosci Remote Sensing*, vol. 49, no. 8, pp. 2918–2923, Aug. 2011.

[5] J. Bellian, C. Kerans, and D. Jennette, "Digital outcrop models: Applications of terrestrial scanning lidar technology in stratigraphic modeling," *Journal of Sedimentary Research*, vol. 75, no. 2, pp. 166–176, Mar. 2005.

[6] S. J. Buckley, J. A. Howell, H. D. Enge, and T. H. Kurz, "Terrestrial laser scanning in geology: data acquisition, processing and accuracy considerations," *Journal of the Geological Society*, vol. 165, no. 3, pp. 625–638, May. 2008.

[7] F. Bretar and N. Chehata, "Terrain modeling from lidar range data in natural landscapes: A predictive and bayesian framework," *IEEE Trans Geosci Remote Sensing*, vol. 48, no. 3, pp. 1568–1578, Mar. 2010.

[8] M. G. Culshaw, "From concept towards reality: developing the attributed 3D geological model of the shallow subsurface," *Quarterly Journal of Engineering Geology and Hydrogeology*, vol. 38, no. 3, pp. 231–384, Aug. 2005.

[9] H. Kessler, S. Mathers, and H. Sobisch, "The capture and dissemination of integrated 3d geospatial knowledge at the british geological survey using gsi3d software and methodology," *Computers & geosciences*, vol. 35, no. 6, pp. 1311–1321, Jun. 2009.

[10] R. Spark and P. Williams, "Digital Terrain Models and the visualization of structural geology," in *Structural Geology and Personal Computers*, ser. Computer Methods in the Geosciences, D. G. de Paor, Ed. Elsevier, 1996, vol. 15, pp. 421–446.

[11] E. A. de Kemp and K. B. Sprague, "Interpretive tools for 3D structural geological modeling parti: Bézier-based curves, ribbons and grip frames," *GeoInformatica*, vol. 7, no. 1, pp. 55–71, 2003.

[12] O. Fernández, J. A. Muñoz, P. Arbués, O. Falivene, and M. Marzo, "Three-dimensional reconstruction of geological surfaces: An example of growth strata and turbidite systems from the ainsa basin (pyrenees, spain)," *AAPG Bulletin*, vol. 88, no. 8, pp. 1049–1068, Aug. 2004.

[13] K. B. Sprague and E. A. de Kemp, "Interpretive tools for 3-D structural geological modelling part II: Surface design from sparse spatial data," *GeoInformatica*, vol. 9, no. 1, pp. 5–32, Mar. 2005.

[14] D. Dhont, P. Luxey, and J. Chorowicz, "3-d modeling of geologic maps from surface data," *AAPG Bulletin*, vol. 89, no. 11, pp. 1465–1474, Nov. 2005.

[15] B. Guillaume, D. Dhont, and S. Brusset, "Three-dimensional geologic imaging and tectonic control on stratigraphic architecture: Upper cretaceous of the tremp basin (south-central pyrenees, spain)," *AAPG Bulletin*, vol. 92, no. 2, pp. 249–269, Feb. 2008.

[16] G. Caumon, P. Collon-Drouaillet, C. le Carlier de Veslud, J. Sausse, and S. Viseur, "Surface-based 3D modeling of geological structures," *Mathematical Geosciences*, vol. 41, no. 8, pp. 927–945, Nov. 2009.

[17] L. Salles, M. Ford, P. Joseph, C. Le Carlier de Veslud, and A. Le Solleuz, "Migration of a synclinal depocentre from turbidite growth strata: the Annot syncline, SE France," *Bulletin de la Societe Geologique de France*, vol. 182, no. 3, pp. 199–220, May. 2011.

[18] T. Frank, A.-L. Tertois, and J.-L. Mallet, "3D-reconstruction of complex geological interfaces from irregularly distributed and noisy point data," *Computers & Geosciences*, vol. 33, no. 7, pp. 932–943, Jul. 2007.

[19] P. Calcagno, J.-P. Chilès, G. Courrioux, and A. Guillen, "Geological modelling from field data and geological knowledge Part I. Modelling method coupling 3D potential-field interpolation and geological rules," *Physics of the Earth and Planetary Interiors*, vol. 171, no. 1-4, pp. 147–157, Dec. 2008.

[20] D. Reif, B. Grasemann, and R. Faber, "Quantitative structural analysis using remote sensing data: Kurdistan, northeast iraq," *AAPG bulletin*, vol. 95, no. 6, pp. 941–956, Jun. 2011.

[21] C. Lajaunie, G. Courrioux, and L. Manuel, "Foliation fields and 3D cartography in geology: principles of a method based on potential interpolation," *Mathematical Geology*, vol. 29, no. 4, pp. 571–584, May. 1997.

[22] J.-P. Chilès, C. Aug, A. Guillen, and T. Lees, "Modelling the geometry of geological units and its uncertainty in 3D from structural data: The potential-field method," in *Proc. Orebody Modelling and Strategic Mine Planning*, 2004, pp. 313–320.

[23] R. Moyen, J.-L. Mallet, T. Frank, B. Leflon, and J.-J. Royer, "3D-parameterization of the 3D geological space - the GeoChron model," in *Proc. European Conference on the Mathematics of Oil Recovery (ECMOR IX)*, 2004.

[24] Ø. Hjelle and S. A. Petersen, "A hamilton–jacobi framework for modeling folds in structural geology," *Mathematical Geosciences*, vol. 43, no. 7, pp. 741–761, Oct. 2011.

[25] J.-P. Chilès and P. Delfiner, *Geostatistics: Modeling Spatial Uncertainty*, ser. Wiley Series in Probability and Statistics. Wiley & Sons, Inc., Hoboken, NJ, USA, Mar. 1999, 696 p.

[26] J. C. Carr, R. K. Beatson, J. Cherrie, T. J. Mitchell, W. R. Fright, B. C. McCallum, and T. R. Evans, "Reconstruction and representation of 3D objects with radial basis functions," in *Proceedings of the 28th annual conference on Computer graphics and interactive techniques*, ser. SIGGRAPH '01. ACM Press, New York, USA, Aug. 2001, pp. 67–76.

[27] E. J. Cowan, R. K. Beatson, H. J. Ross, W. R. Fright, T. J. McLennan, T. R. Evans, J. C. Carr, R. G. Lane, D. V. Bright, A. J. Gillman, P. A. Oshust, and M. Titley, "Practical implicit geological modeling," in *Proc. 5th International Mining Conference*, S. Dominy, Ed. Australian Inst. Mining and Metallurgy, 2003, pp. 89–99.

[28] L. Greengard and V. Rokhlin, "A fast algorithm for particle simulations," *Journal of Computational Physics*, vol. 73, no. 2, pp. 325–348, Dec. 1987.

[29] W. E. Lorensen and H. E. Cline, "Marching cubes: a high resolution 3d surface construction algorithm," *SIGGRAPH Comput. Graph.*, vol. 21, no. 4, pp. 163–170, Aug. 1987.

[30] D. Ledez, "Euclidean distance mapping: Geological applications," in *Terra Nostra, (Proceedings of IAMG)*, vol. 04. Proc. IAMG, Berlin, September 2002, pp. 25–30.

[31] A. Sharf, T. Lewiner, G. Shklarski, S. Toledo, and D. Cohen-Or, "Interactive topology-aware surface reconstruction," *ACM Trans. Graph.*, vol. 26, no. 3, p. 43, Jul. 2007.

[32] F. Lepage, "Génération de maillages tridimentionnels pour la simulation des phénomènes physiques en géosciences," Ph.D. dissertation, INPL, Nancy, France, 2003.

[33] H. Si, "Constrained delaunay tetrahedral mesh generation and refinement," *Finite Elements in Analysis and Design*, vol. 46, no. 1-2, pp. 33–46, Jan. 2010.

[34] G. Caumon, C. H. Sword, and J.-L. Mallet, "Building and editing a Sealed Geological Model," *Mathematical Geology*, vol. 36, no. 4, pp. 405–424, May. 2004.

[35] P. Durand-Riard, G. Caumon, and P. Muron, "Balanced restoration of geological volumes with relaxed meshing constraints," *Computers & Geosciences*, vol. 36, no. 4, pp. 441–452, Apr. 2010.

[36] P. Durand-Riard, L. Salles, M. Ford, G. Caumon, and J. Pellerin, "Understanding the evolution of synsedimentary faults: coupling decompaction and 3d sequential restoration," *Marine and Petroleum Geology*, vol. 28, no. 8, pp. 1530–1539, Aug. 2011.

[37] J.-L. Mallet, "Space-time mathematical framework for sedimentary geology," *Mathematical geology*, vol. 36, no. 1, pp. 1–32, Jan. 2004.

[38] N. Cherpeau, G. Caumon, and B. Levy, "Stochastic simulations of fault networks in 3D structural modeling," *C.R. Académie des Sciences. Géosciences*, vol. 342, no. 9, pp. 687–694, Sep. 2010.

[39] A.-L. Tertois and J.-L. Mallet, "Editing faults within tetrahedral volumes in real time," in *Structurally Complex Reservoirs*, ser. Geological Society, London, Special Publications, S. Jolley, D. Barr, J. Walsh, and R. Knipe, Eds., 2007, vol. 292, pp. 89–101.

[40] L. M. Mitre-Salazar, "Las imágenes landsat - una herramienta útil en la interpretación geologico estructural; un ejemplo en el noreste de méxico," *Revista mexicana de ciencias Geológicas*, vol. 5, no. 1, pp. 37–46, 1981.

[41] M. G. Rowan, T. F. Lawton, K. A. Giles, and R. A. Ratliff, "Near-salt deformation in la popa basin, mexico, and the northern gulf of mexico: A general model for passive diapirism," *AAPG Bulletin*, vol. 87, no. 5, pp. 733–756, May. 2003.

[42] K. A. Giles and T. F. Lawton, "Attributes and evolution of an exhumed salt weld, la popa basin, northeastern mexico," *Geology*, vol. 27, no. 4, pp. 323–326, 1999.

[43] K. A. Giles and T. F. Lawton, "Halokinetic sequence stratigraphy adjacent to El Papalote Diapir, La Popa Basin, Northeastern Mexico," *AAPG Bulletin*, vol. 86, no. 5, pp. 823–840, May. 2002.

[44] D. Kudelski, J. Mari, and S. Viseur, "3d feature line detection based on vertex labeling and 2d skeletonization," in *Shape Modeling International Conference (SMI), 2010.* IEEE, Jun. 2010, pp. 246–250.

[45] R. You and B. Lin, "A quality prediction method for building model reconstruction using lidar data and topographic maps," *IEEE Trans Geosci Remote Sensing*, vol. 49, no. 9, pp. 3471–3480, Sep. 2011.

[46] A. Katartzis and H. Sahli, "A stochastic framework for the identification of building rooftops using a single remote sensing image," *IEEE Trans Geosci Remote Sensing*, vol. 46, no. 1, pp. 259–271, Jan. 2008.

[47] N. Cherpeau, G. Caumon, J. Caers, and B. Levy, "Method for stochastic inverse modeling of fault geometry and connectivity using flow data," *Mathematical Geosciences*, vol. 44, no. 2, pp. 147–168, Feb. 2012.

Guillaume Caumon received a Master from the Nancy School of Geology (ENSG) in 1999 and a PhD in Geosciences from INPL in 2003. He was a postdoctoral scholar at Stanford University in 2003-2004. He currently is a Professor in Geomodeling at the Université de Lorraine - ENSG where he has been leading the Gocad Consortium since 2007. His main research interests concern the modeling, visualization and processing of geological objects in the face of uncertainty. In 2009, he received the Vistellius Award from the IAMG.

Gary Gray obtained a PhD in Structural Geology from the University of Texas at Austin in 1985. He has spent the last 27 years at ExxonMobil Upstream Research Company in Houston, Texas. He has broad experience in many basins around the world with a particular interest in the geology of NE Mexico and structural modeling.

Christophe Antoine received a DESS (MSc) in computer engineering from the University of Nancy in 1992. He then worked as research engineer on automatic speech recognition at LORIA (Lorraine Research Laboratory in Computer Science and its Applications) and was a senior engineer with DIALOCA (automatic speech recognition software company). He joined the Gocad Research Group as research engineer in 2007.

Marc-Olivier Titeux received his Master Degree from the School Matmeca (University of Bordeaux 1) in 2004. He obtained a PhD in Geosciences from INPL in 2009. During 2009-2011, he was a post-doctoral researcher at the University of Texas at Austin. His research focuses on structural restoration, upscaling of mechanical properties, and the mechanical characterization of karst collapses. He is now working with IFPEn on structural restoration and fluid flow modeling in deeply buried reservoirs.